Progress on new methods, materials, and insights for safety Li-ion battery systems

Donal Finegan

NASA Battery Safety Workshop

18 Nov 2020

Co-investigators:

NREL: Matt Sharp, Julia Billman, Qibo Li, Chuanbo Yang, Matt Keyser

NASA: Eric Darcy, Will Walker, John Darst

UCL: Paul Shearing, Martin Pham, Tom Heenan

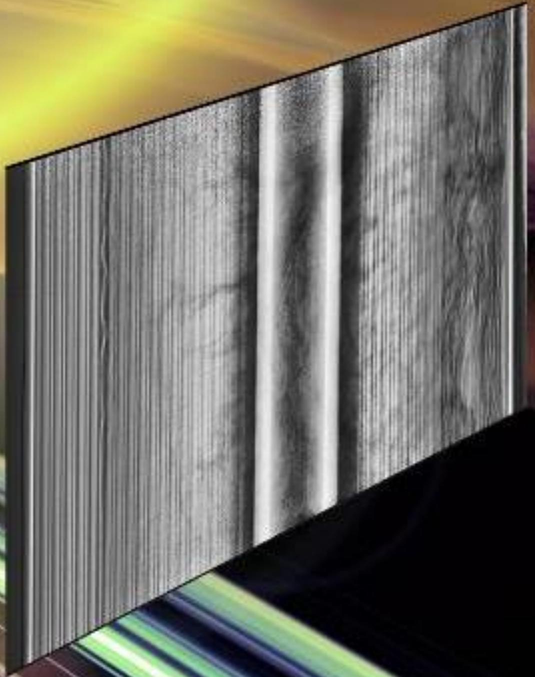

Contents

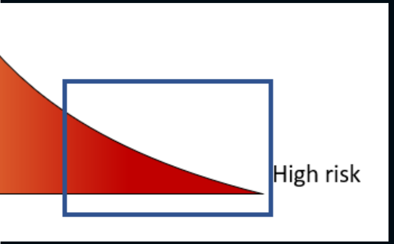

High-risk failure mechanisms


Bursting: Top


Bursting: Bottom

18650 cells


Breach: Top


Breach: Top


Breach: Side


Breach: Side


Breach: Bot


Breach: Bot

Hazardous flare stemming from breach


Image courtesy of E. Darcy (NASA)

Most challenging failure mechanism to handle

Characterizing breaching mechanism

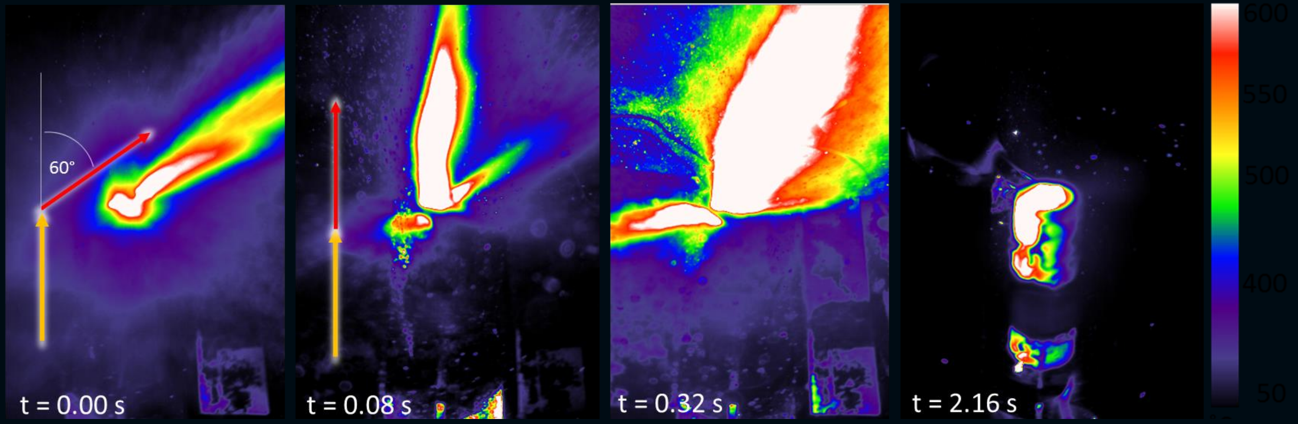

Breach: Top

Cell type: Li-ion 18650
Capacity: 3.4 Ah
State of Charge: 100 % (4.2 V)
Bottom vent: Yes
Wall thickness: 220 µm
Orientation of cell: Positive end up
Location of ISCD radially: 6 winds in
Location of ISCD longitudinally: Top
Side of ISCD in image: Right

Location of FOV longitudinally: Top
Frame rate: 2000 Hz
Frame dimension (Hor x Ver): 1822 x 1140 pixels
Pixel size: 10 µm

Cause of breach

- Reacting material fluidizes and flows towards the top vent
- Material deflects off the spin-groove, causing thermal stress
- The spin-groove melts leading to a breach and escape of hot material

Selective Positioning of the ISC Device

NATIONAL RENEWABLE ENERGY LABORATORY

Internal short-circuiting device

- 18650 cells were manufactured with the ISC device placed at **3 different longitudinal locations**

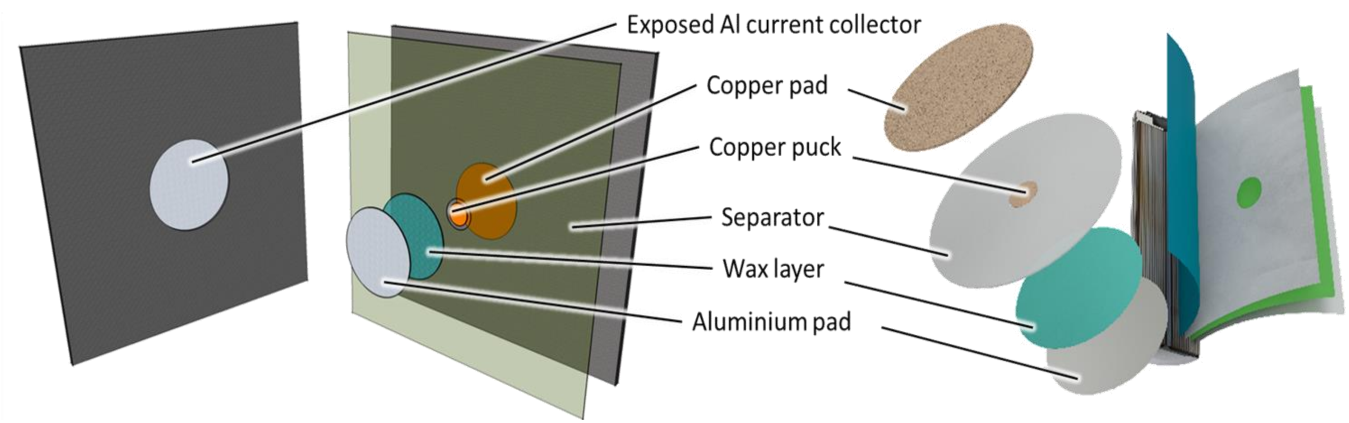

ISC at bottom

ISC at top

ISC at midway

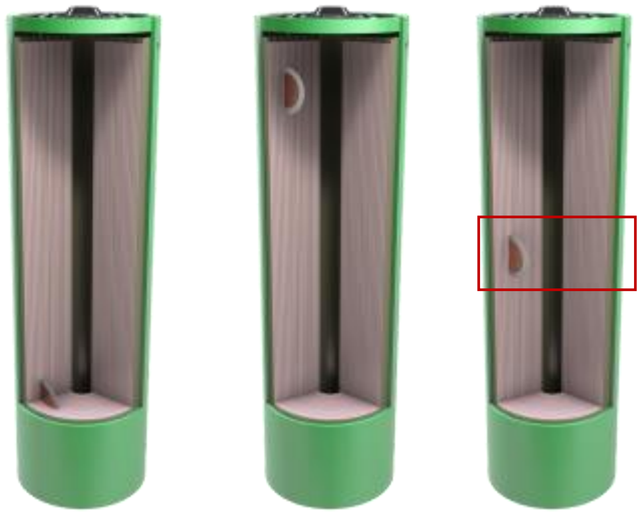

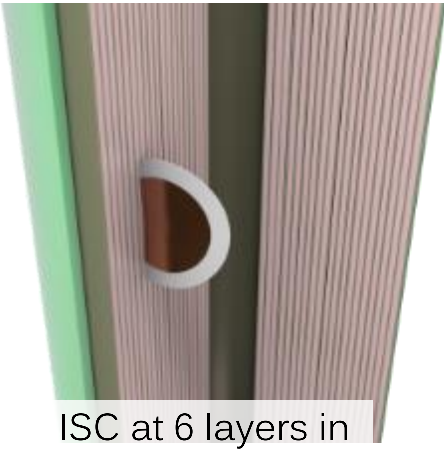

Risk map

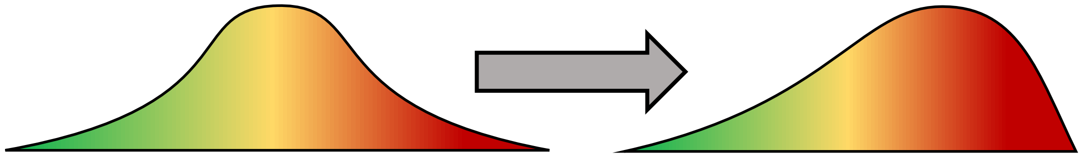

From a study of 200 cells, the propensity of cell to undergo certain failure mechanisms, under certain conditions, was mapped.

The number in each box represents the fraction of cells of that particular design, to undergo a particular failure mechanism

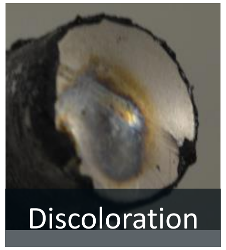

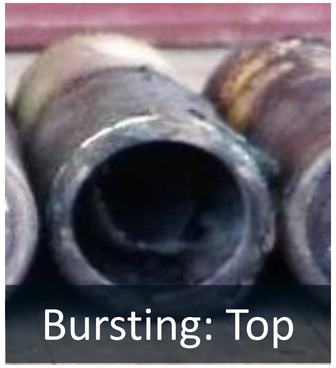

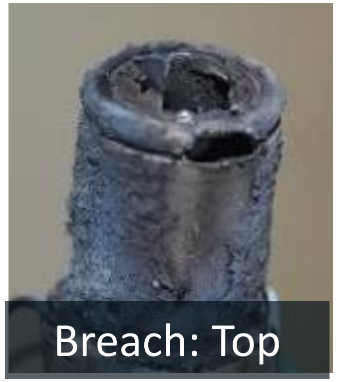

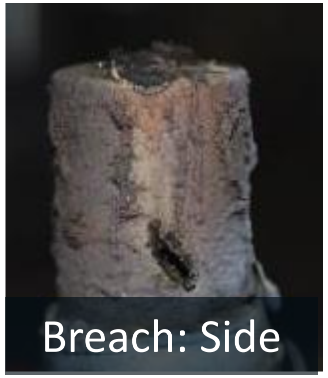

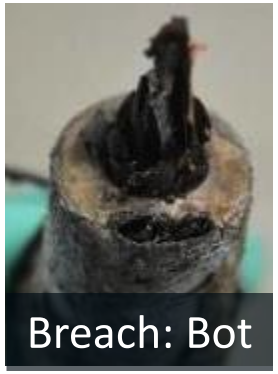

ISC Position	Design	Total	Bursting		Breach			Contained
			Top	Bot	Top	Side	Bot	
None	220 µm, BV	45	0.00	1.00	0.00	0.00	0.44	0.00
None	220 µm, NBV	46	0.02	0.00	0.07	0.02	0.16	0.98
None	250 µm, NBV	43	0.00	0.00	0.07	0.00	0.00	1.00
Top	220 µm, BV	11	0.09	0.27	0.64	0.00	0.27	0.64
Mid	220 µm, BV	13	0.08	0.54	0.08	0.00	0.62	0.38
Bot	220 µm, BV	12	0.00	1.00	0.00	0.17	1.00	0.00
Top	250 µm, NBV	9	0.00	0.00	0.56	0.00	0.00	1.00
Mid	250 µm, NBV	7	0.00	0.00	0.43	0.14	0.43	1.00
Bot	250 µm, NBV	8	0.00	0.00	0.38	0.13	0.25	1.00

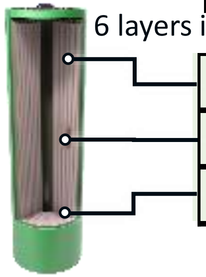

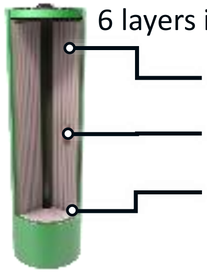

Finegan et al., Modelling and experiments to identify high-risk failure scenarios for testing the safety of lithium-ion cells, *J. of Power Sources*, **2019**

Key findings:

1. Proximity of the ISC device to either end increases the risk of breach/ bursting at that end.
2. Thicker casings reduce the risk of bursting but have a similar risk of breaching.
3. Bottom vents reduce the risk of breaching overall, but increase the risk of bottom breaching.

Fractional thermal runaway calorimeter (FTRC)

NREL
NATIONAL RENEWABLE ENERGY LABORATORY

Ejected and non-ejected heat output

- 3.6 Ah 18650 cells
- Location of thermal runaway initiation **does not have significant impact on total heat output**, but does **influence the fraction of heat ejected**
- Around **70% of heat is ejected**, mostly through the positive vent
- Initiation near the bottom increases risk of bottom breach and heat from the bottom

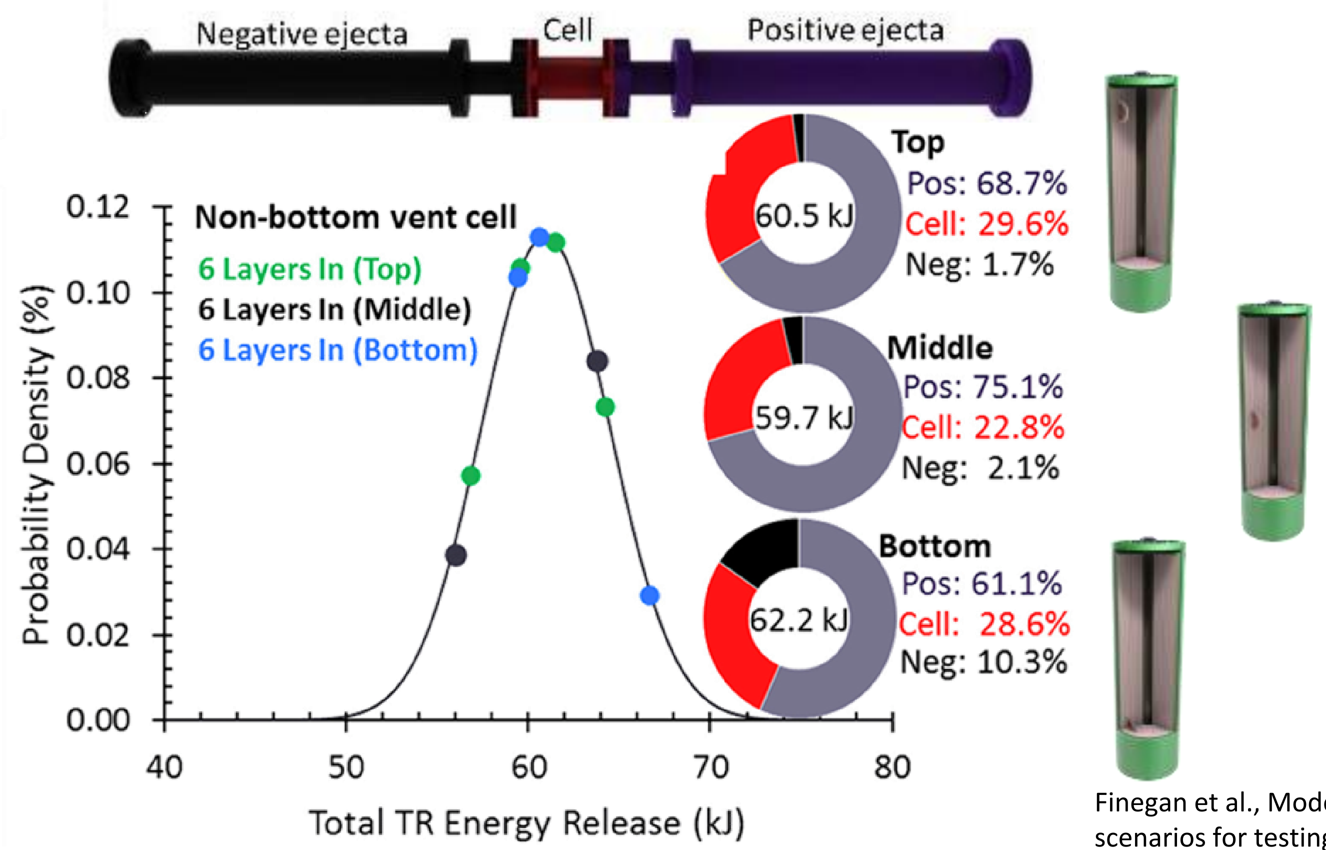

Finegan et al., Modelling and experiments to identify high-risk failure scenarios for testing the safety of lithium-ion cells, *J. of Power Sources*, **2019**

Thermal stress and bursting pressure

Surface temperature and burst pressure

- The **highest risk** scenarios for pressure-induced breaches are when initiation of **thermal runaway occurs near either end of the 18650 cell**.
- Bust pressures can reach < 1.5 MPa for temperatures > 650 °C.
- If a cell produces 6 L of gas, and is clogged, the internal pressure could reach 30 Mpa..

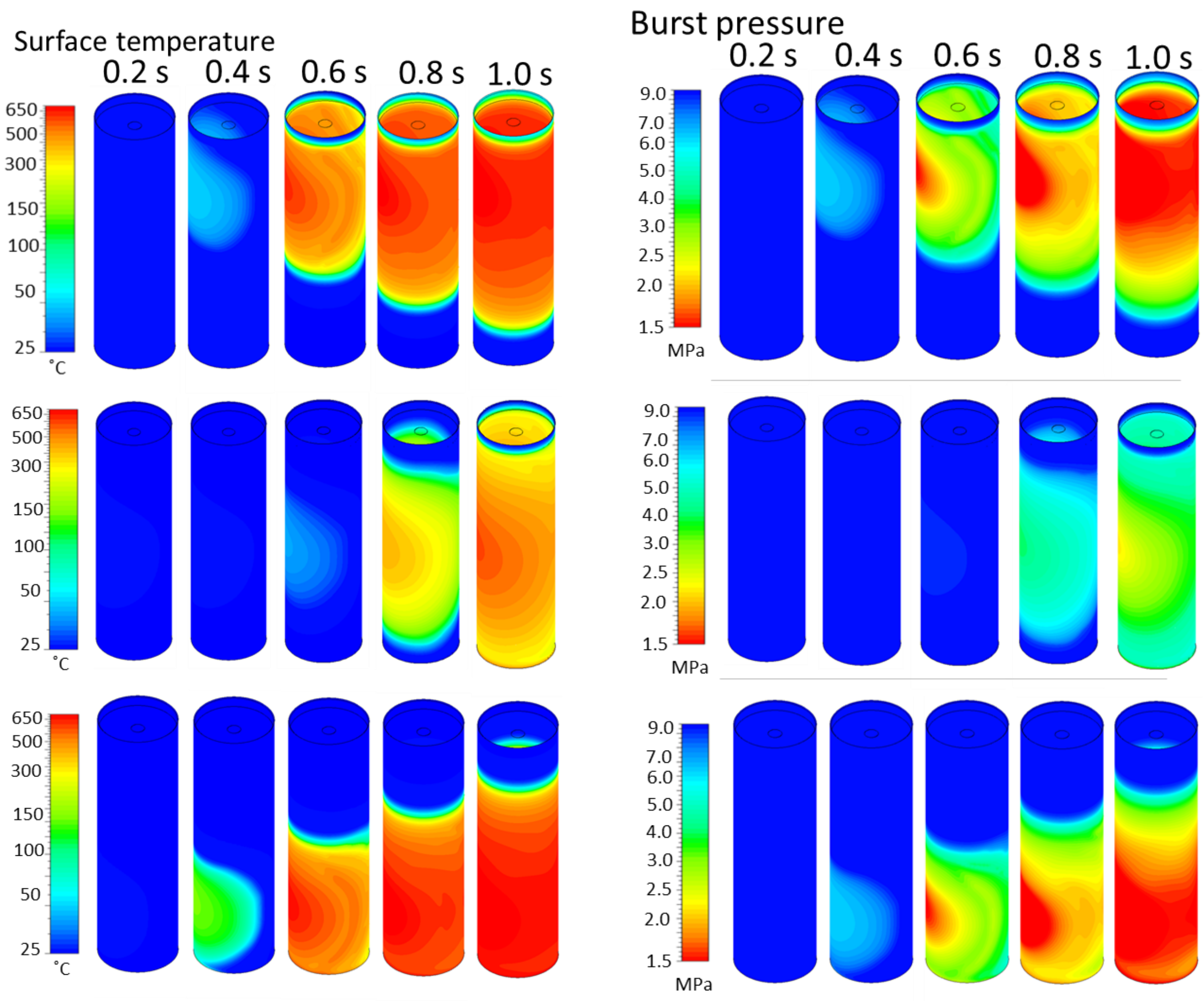


Breach: Top

Explains increased risk of breaching occurring, but not the consistent location at spin groove

Based on tensile strength properties for S350GD mild steel

Results guiding safe battery designs

- **Single cell data applied to battery pack simulations**
  - Modelling sizing of heat sinks to avoid propagation
  - Estimating temperatures of pack enclosures when subject to ejected heat
  - Spatially quantifying the distribution of heat within an enclosure following cell failure

Heat sink sizing

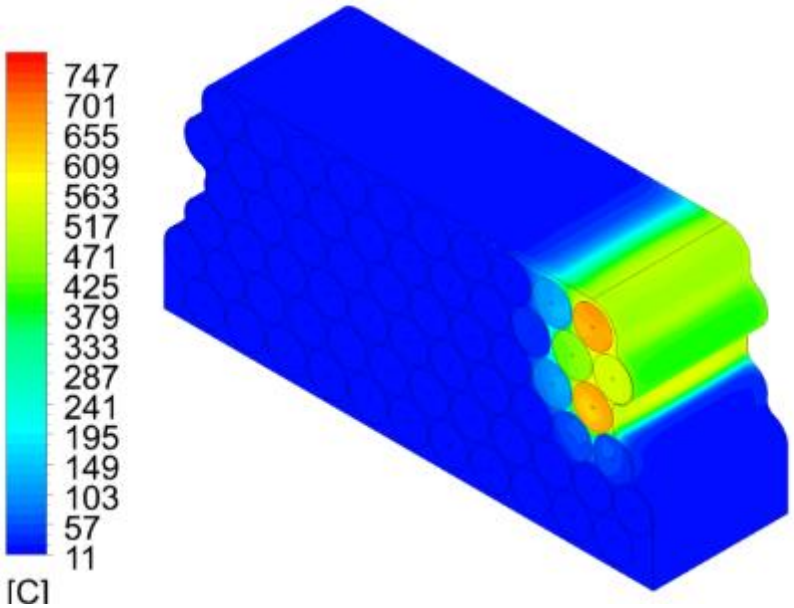

Enclosure (can) subject to ejected heat

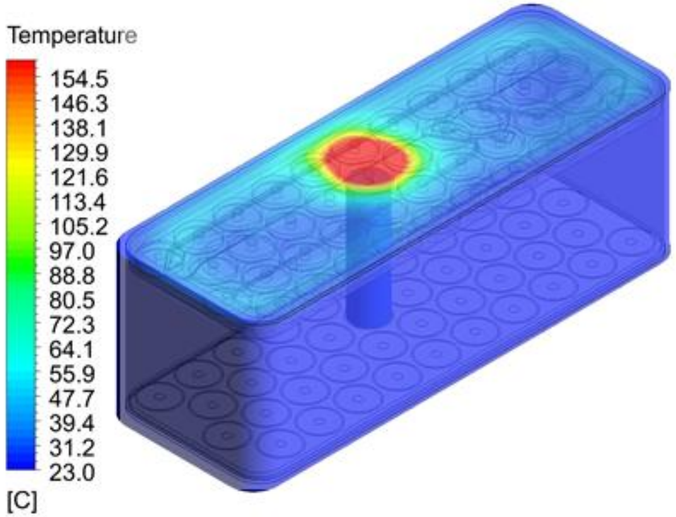

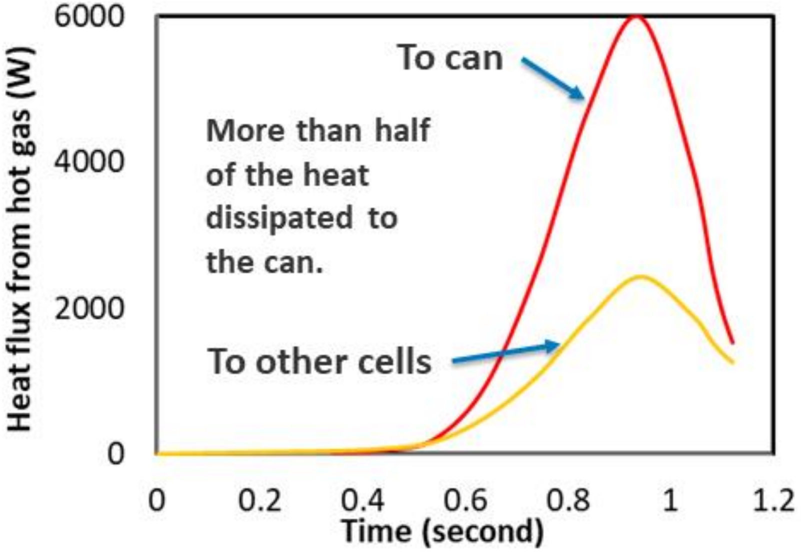

Work by Chuanbo Yang (NREL)

Results guiding safe battery designs

NASA X57 electric aircraft

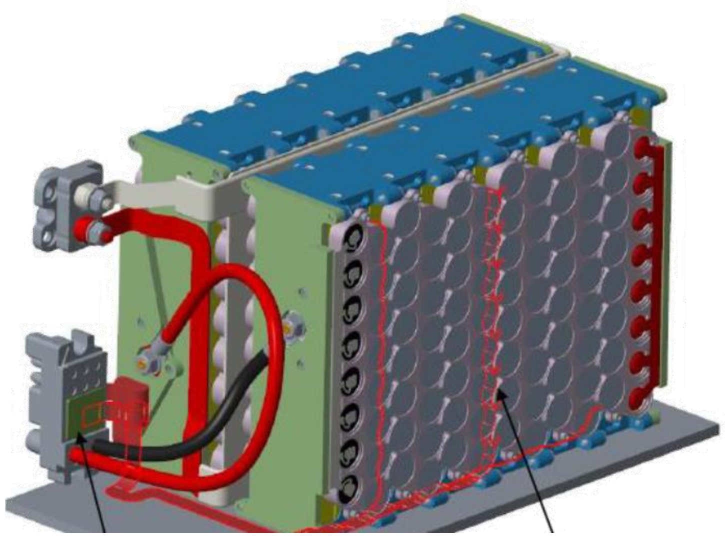

Eric Darcy and team at Johnson Space Center

Battery failure databank

- Radiography and thermal data from over 300 tests of commercial cells
    - Providing engineers and researchers with data to inform models
- Link internal phenomena with external risks
- Compare heat output and mass ejection from different abuse mechanicals
    - Nail penetration
    - Thermal abuse
    - Internal short circuiting
- Compare different models of cells
    - Power cells
    - Energy cells

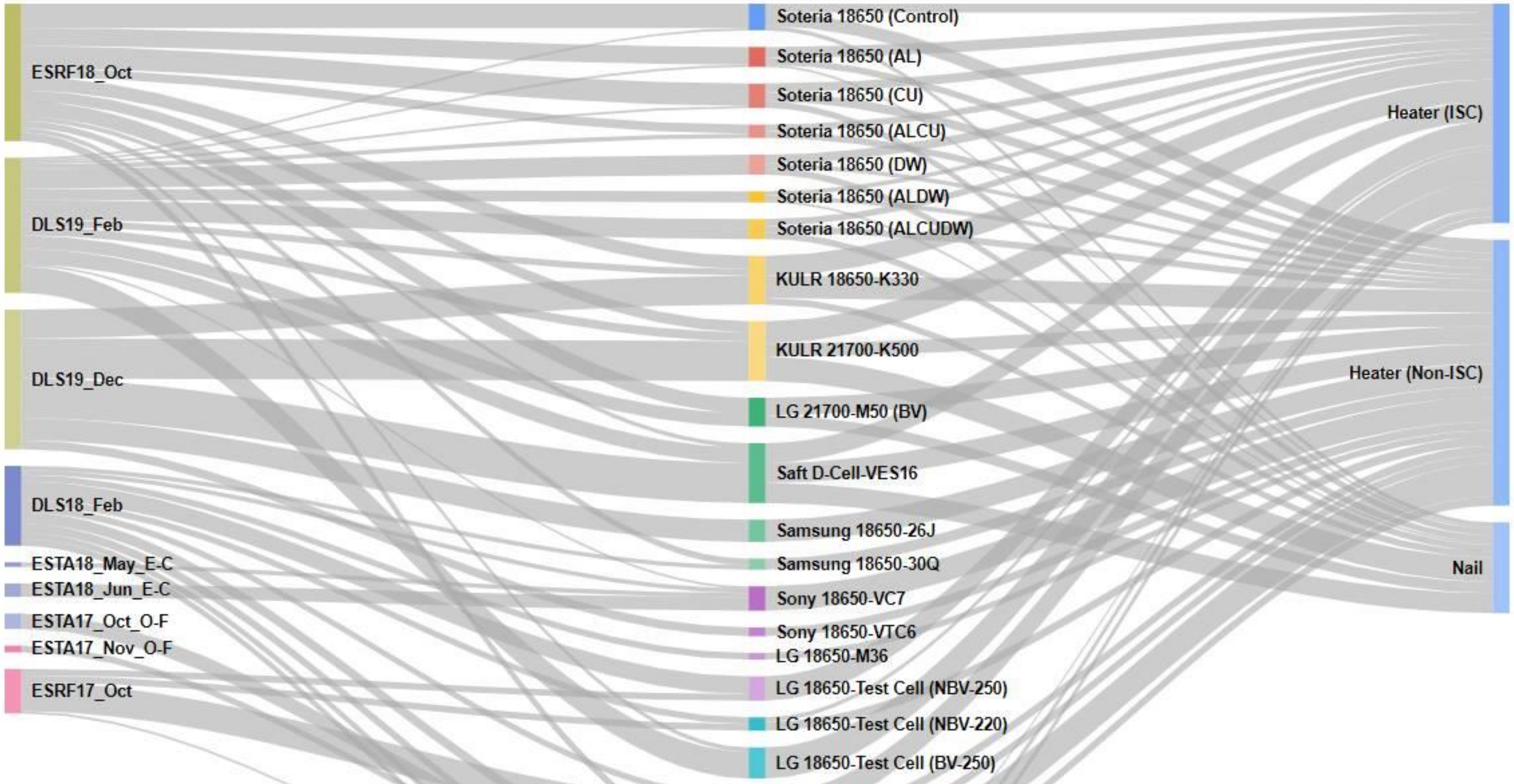

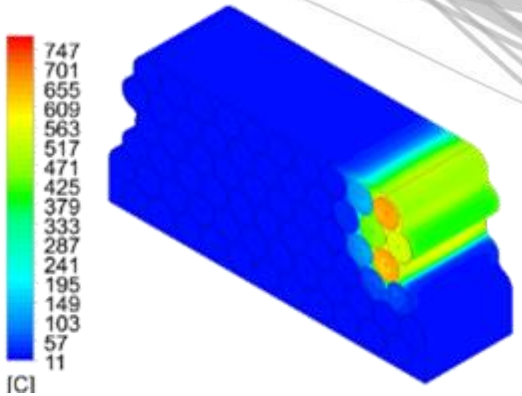

DLS – Diamond Light Source
ESRF – European Synchrotron Radiation Facility

Contents

Acoustic Time of Flight - Introduction

- Rapid in-line, non-destructive cell diagnostic technique
- High-frequency pulse-echo mechanism to evaluate electrode level changes

Attenuation

$$\Delta Z = \sqrt{|\Delta\rho| K}$$

Velocity

$$v = \sqrt{\frac{K}{\rho}}$$

- Time of flight dependent on:
  - Material density
  - Material elastic modulus
  - Thickness
  - Structural changes

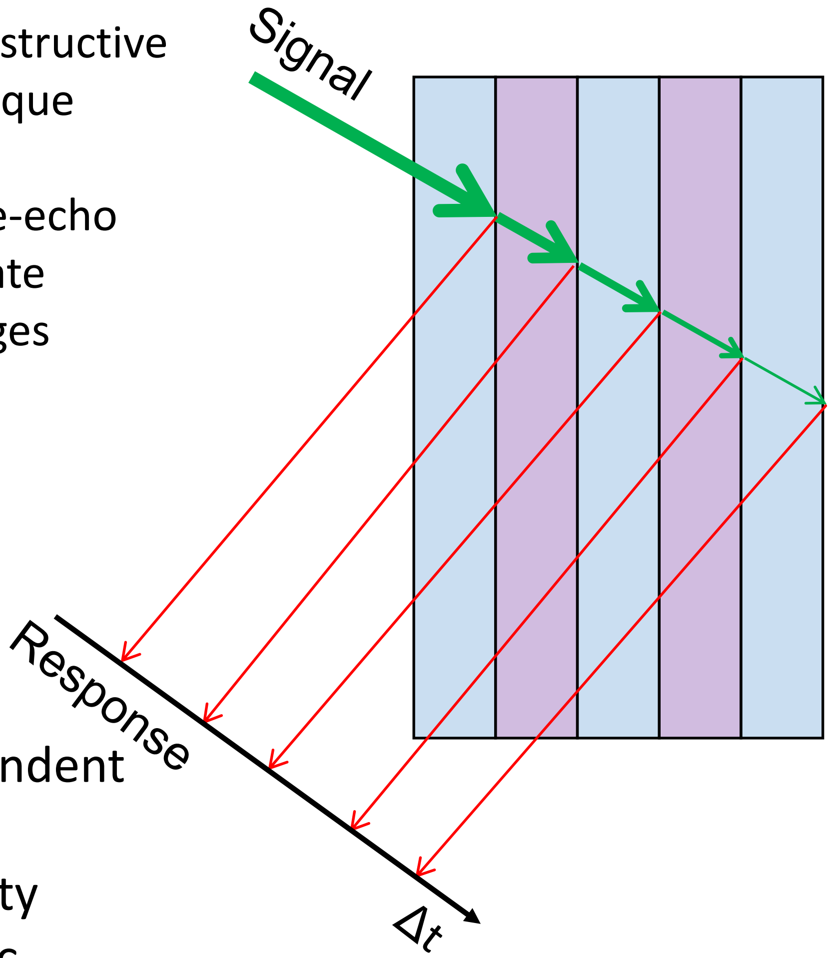

Figure 1: Illustrating the fundamental principles of acoustic time of flight

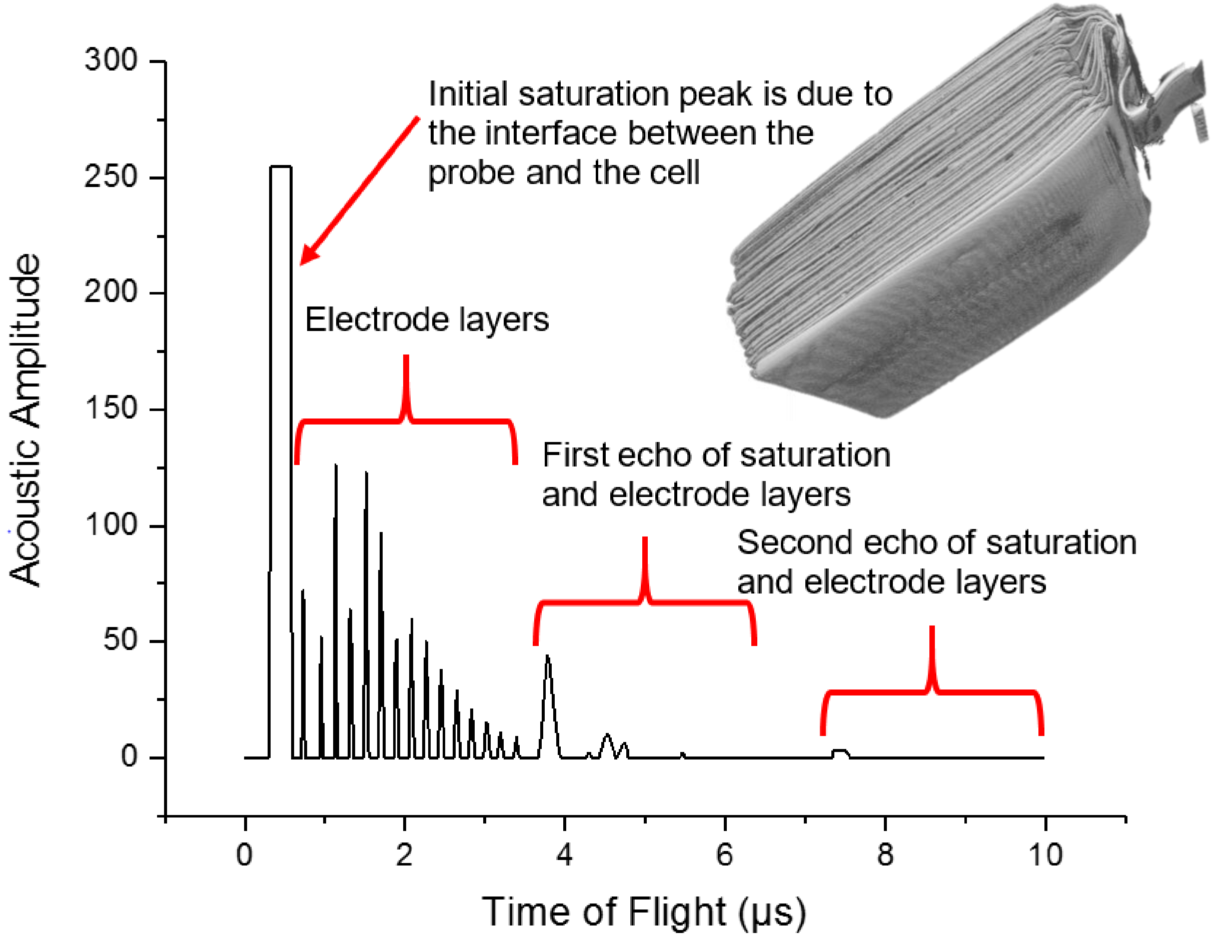

Figure 2: Representation of a characteristic acoustic time of flight waveform for a pouch cell, CT of corresponding pouch cell shown inset

Acoustic Time of Flight - Introduction

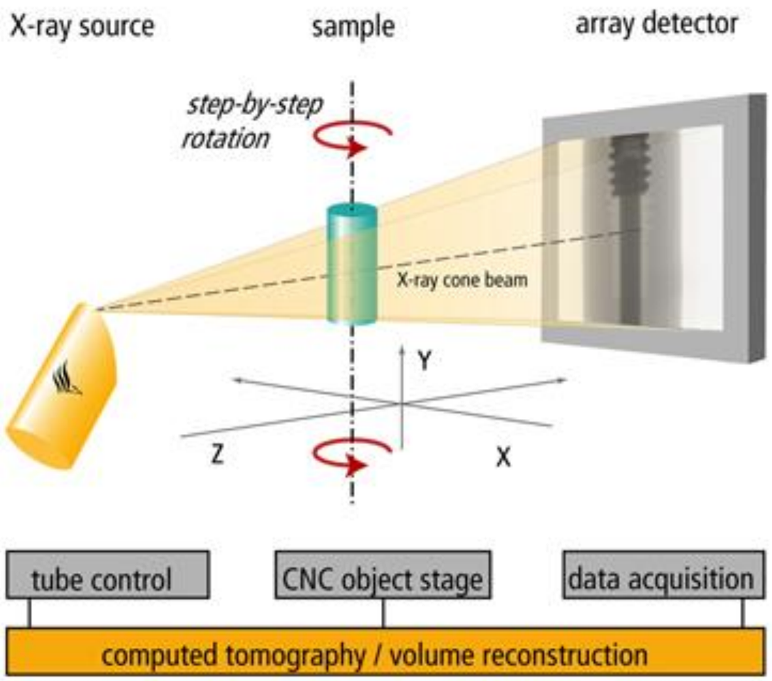

Figure 3: A simple schematic of the experimental set-up used in the Nikon XT H225 to produce simultaneous acoustic spectroscopy and X-ray imaging.

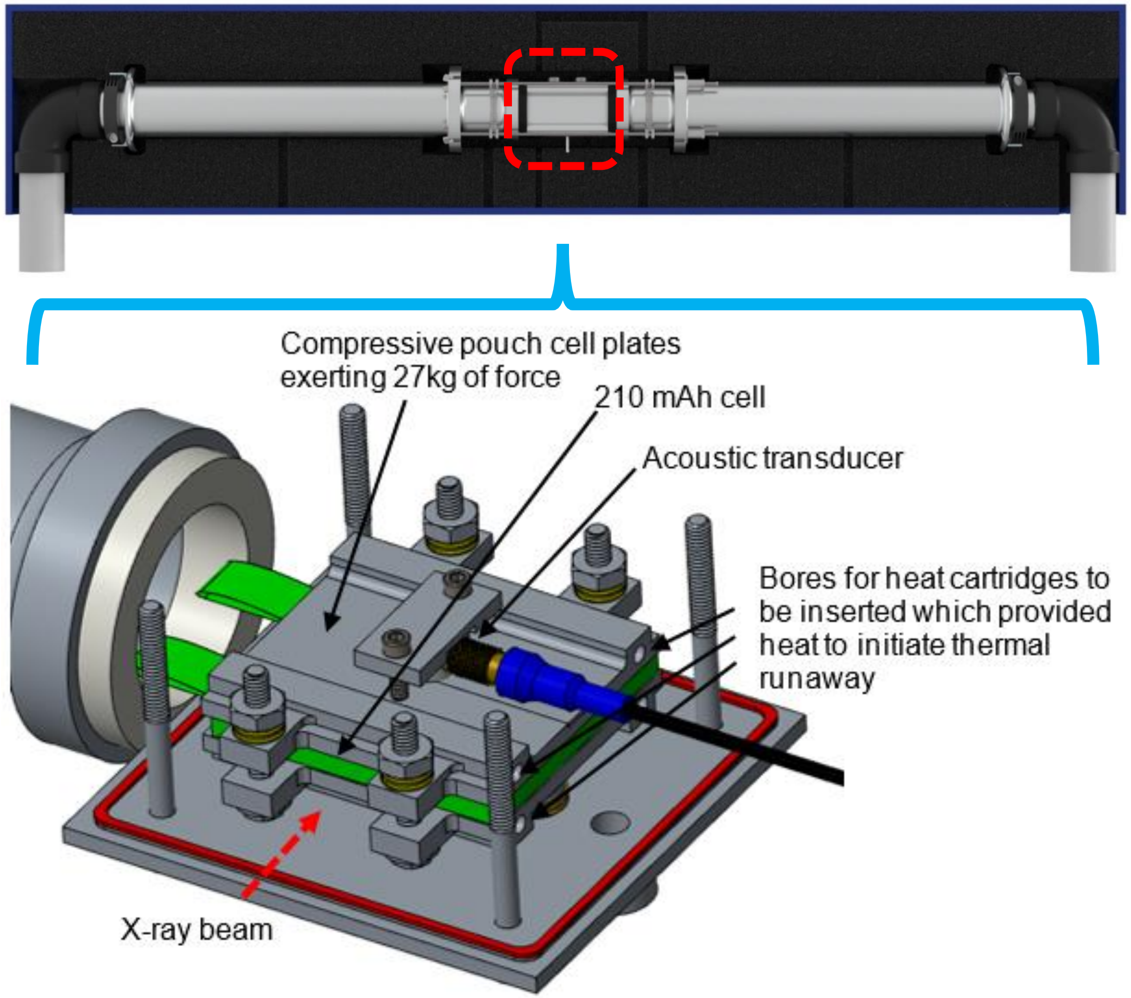

Figure 4: CAD rendering of the ultrasonic transducer in the pouch cell calorimeter cell chamber stack under compression

XCT – Defect Detection

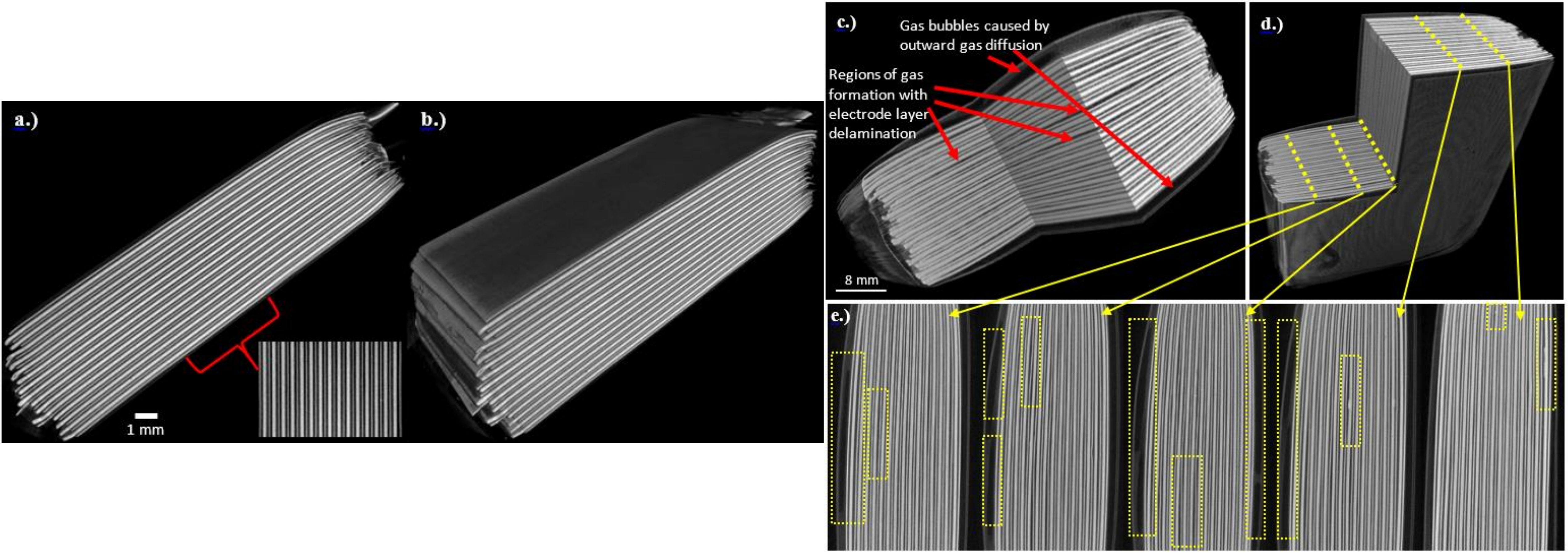

Figure 7: (a,b) Pre- and (c, d, e,) post- mortem XCT of defect driven delaminations in a commercial Li-ion cell

Acoustic Time of Flight – Defect Detection

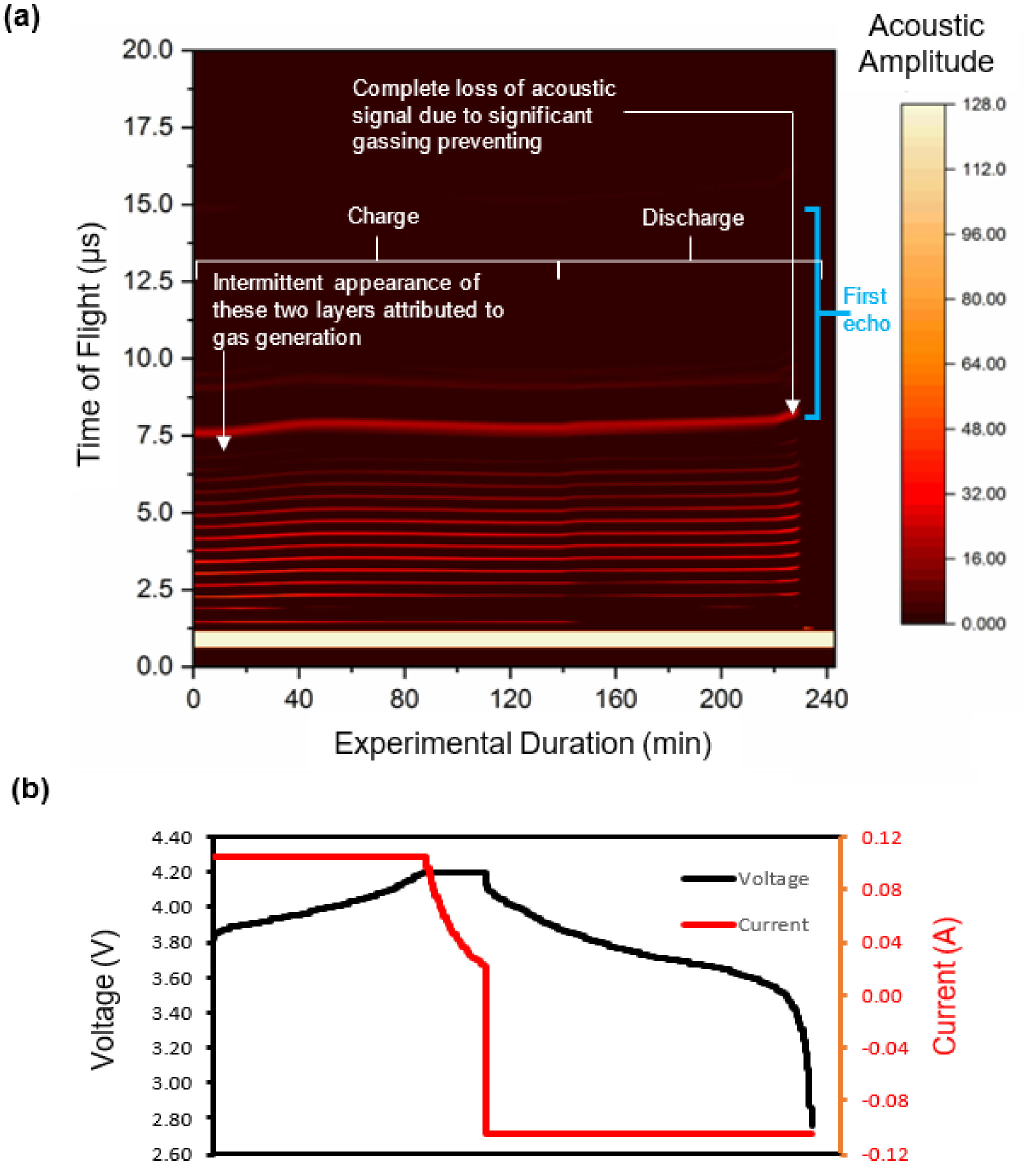

Instantaneous acoustic pulse-echo 'snapshot' acquisition, at Experimental Duration = 0 min

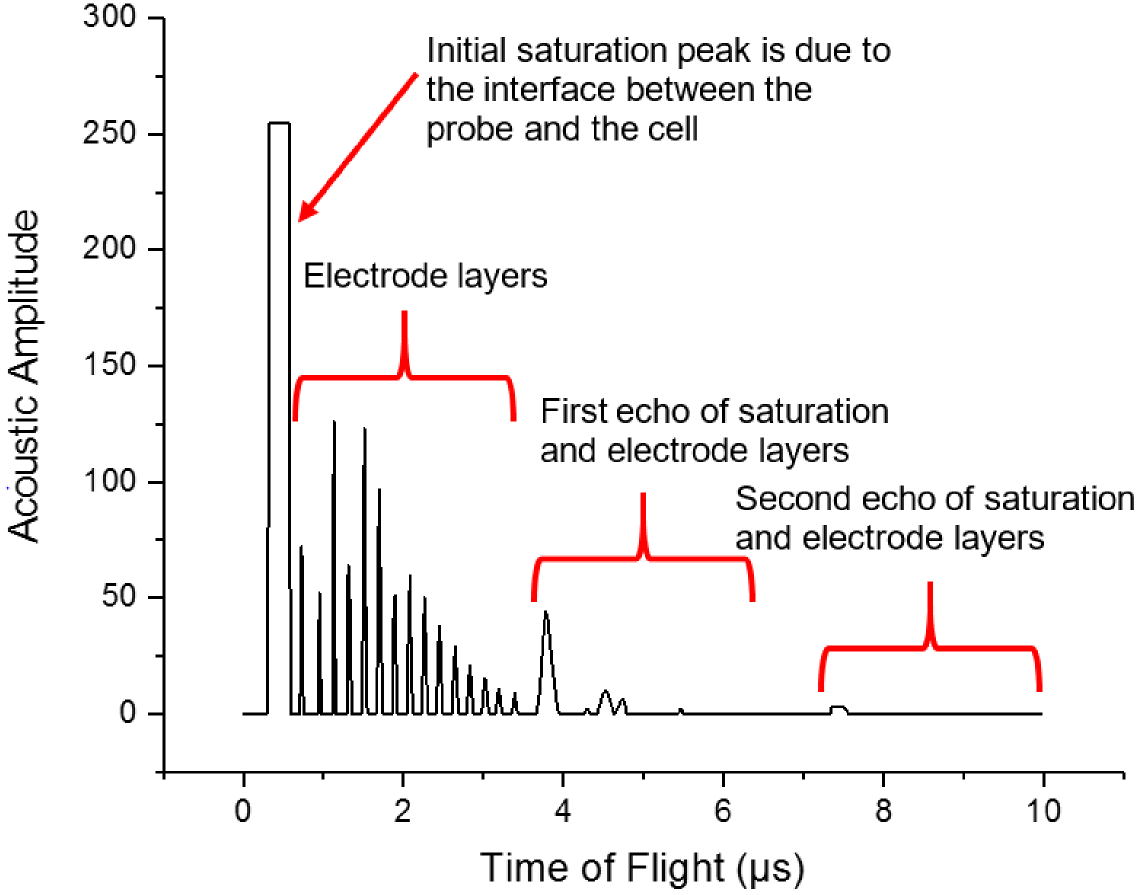

Figure 5: Acoustic time of flight during defect induced delamination during operation of a 210 mAh pouch cell.

Acoustic Time of Flight – Thermal Runaway

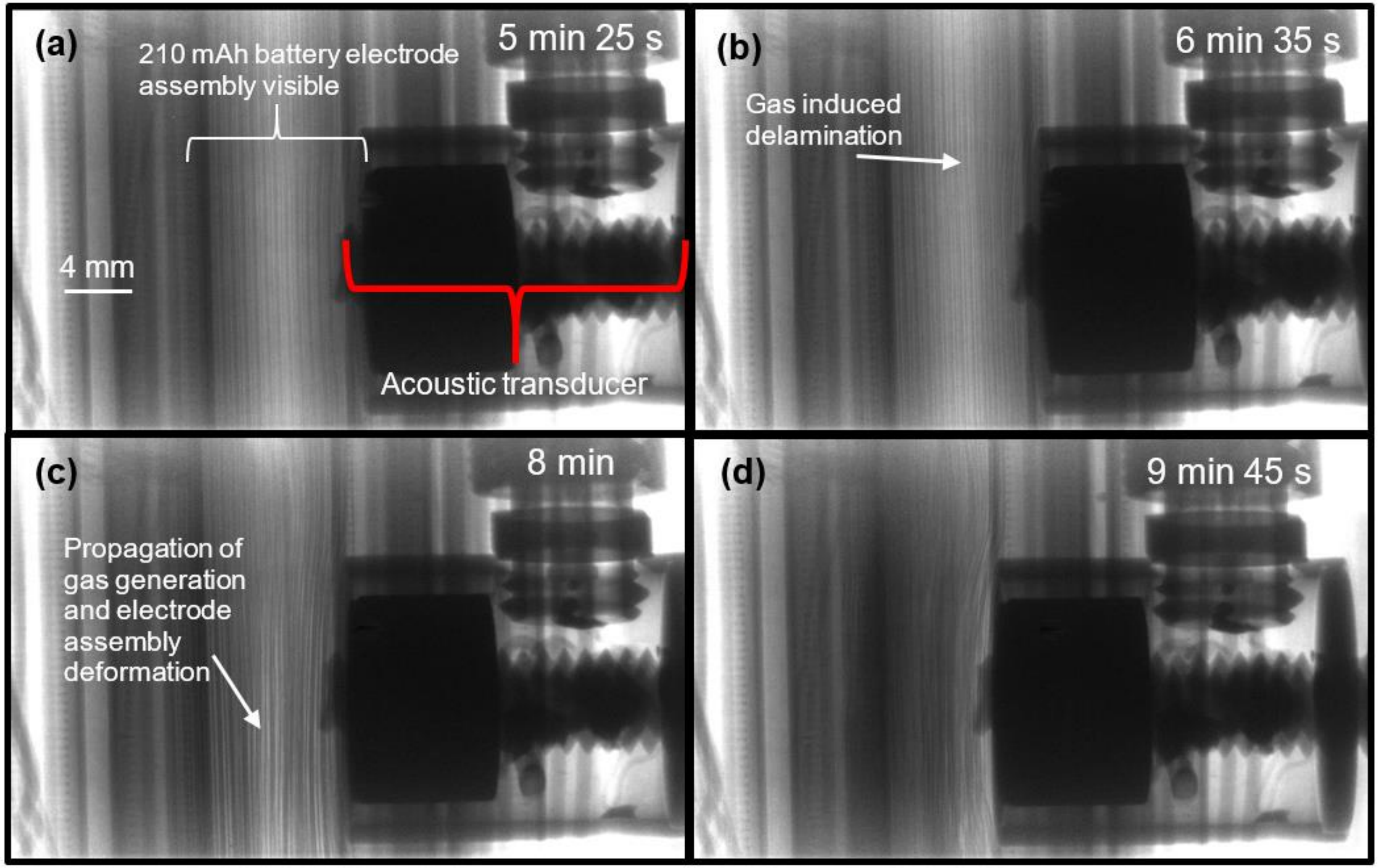

Figure 8: Selected radiography frames from Cell 1 highlighting significant structural changes during thermal runaway in the first failure test. Delamination and gas generation predicated the initiation of widespread thermal runaway.

Acoustic Time of Flight – Thermal Runaway

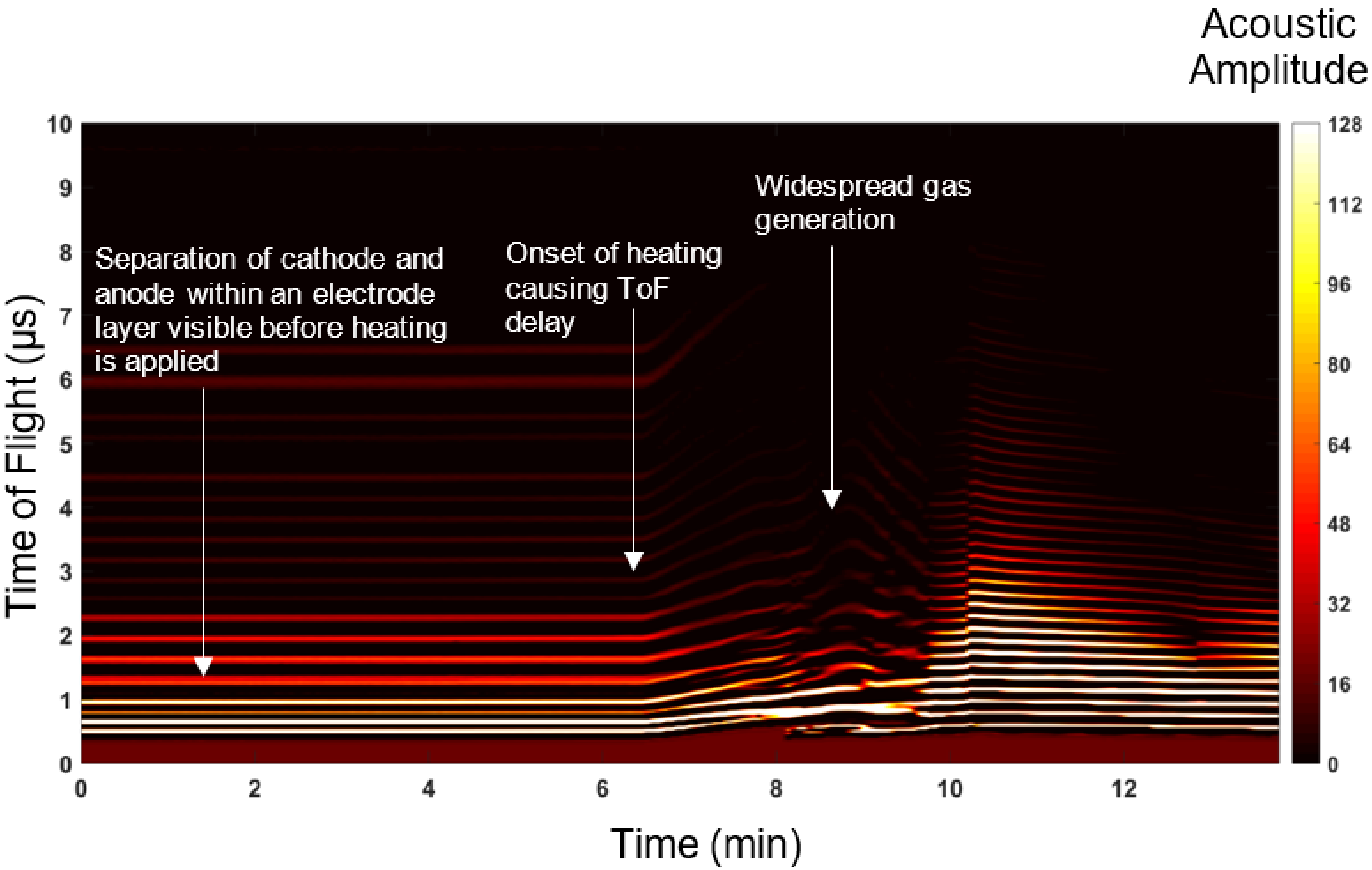

Figure 9: Acoustic time of flight during thermal runaway of Cell 1

Contents

PCCs: Thermal Runaway Mechanisms

- Anode and cathode contact via the nail causes an unmitigated short-circuit

- Elevated temperatures due to Joule heating causes thermal decomposition of electrode components, initially with the polyolefin separator and electrolyte

- In cells with the PCC, the PCC would react to the elevated temperatures before the separator could fail, this would prevent cathode-anode contact as well as electrically isolating the cathode from the nail and the anode.

- Whether the PCC's safety mechanism acted before the failure of the 10 µm polypropylene separator would dictate the efficacy of the PCC.

Typical cell failure from nail penetration

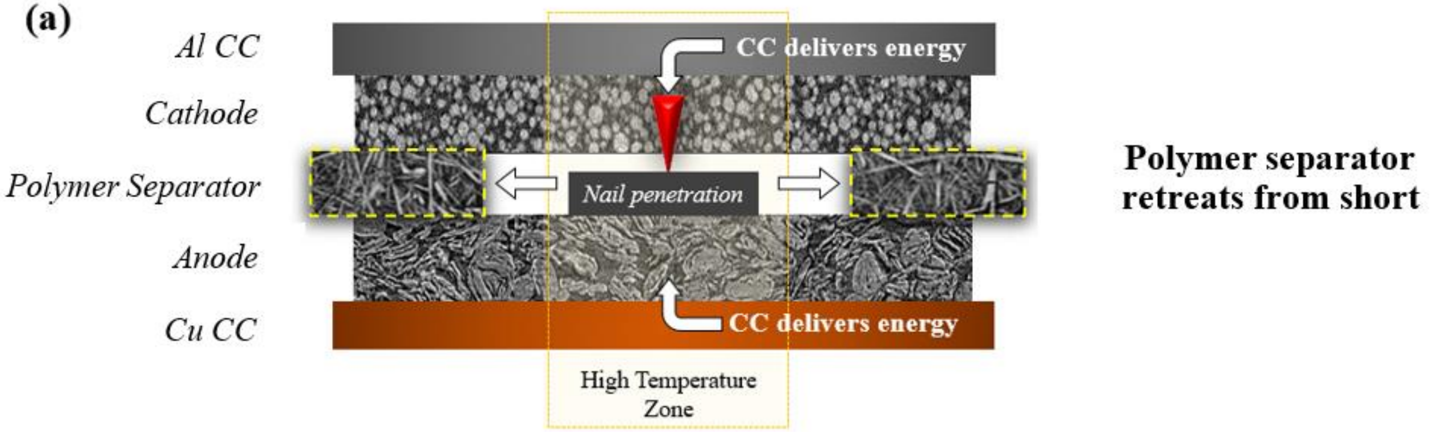

PCC thermal runaway prevention mechanism

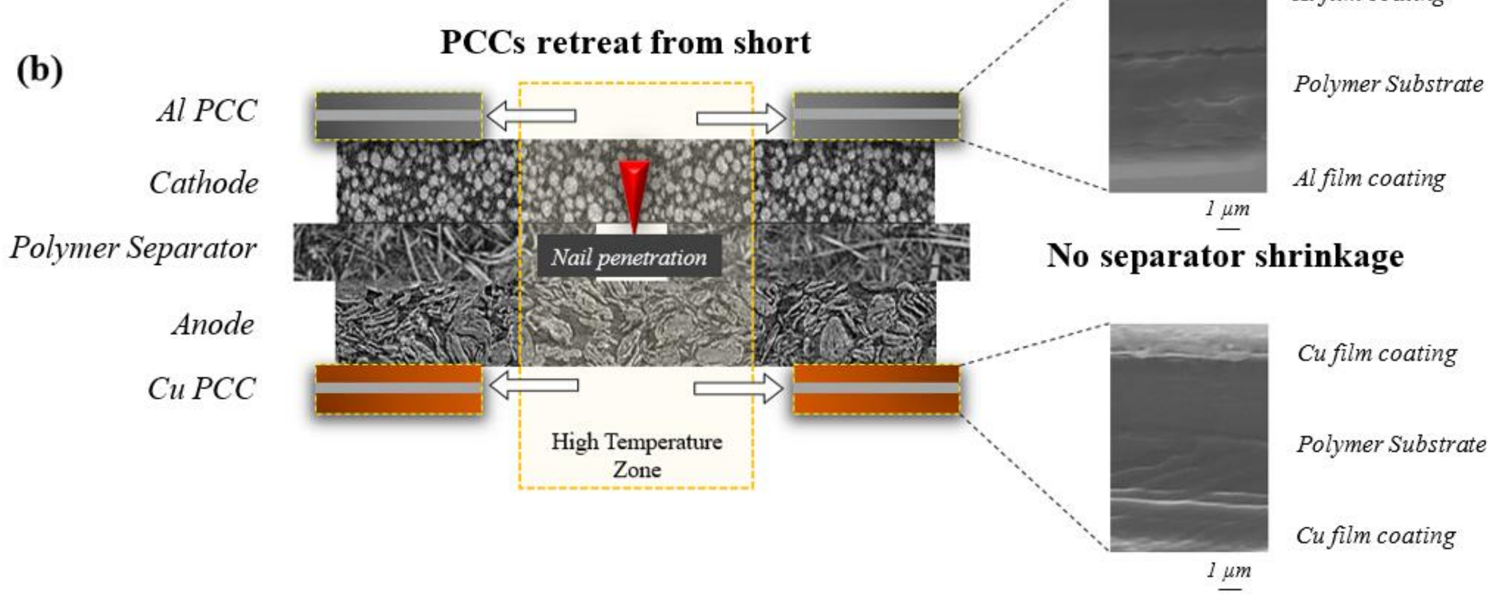

PCCs: Gravimetric Energy Density

- Similar thicknesses to commercial metal foil current collectors (CCs):
  - Al CC: 15 µm, Al PCC: 11 µm
  - Cu CC: 10 µm, Cu PCC: 11 µm
- PCCs have a polymer substrate (ca. 8 µm thickness) with ca. 0.5 µm metal film coating of Al or Cu
- Therefore, a significant reduction in the amount of metal required by the PCC compared to commercial metal foils used as current collectors
- This reduction in metal is noticeable on the cell level as the average mass reduction was 2.2 grams, ca. 5% of total mass of a commercial metal foil CC control cell
- Mechanical properties of PCCs allow for assimilation with current cylindrical cell roll-to-roll manufacturing technology

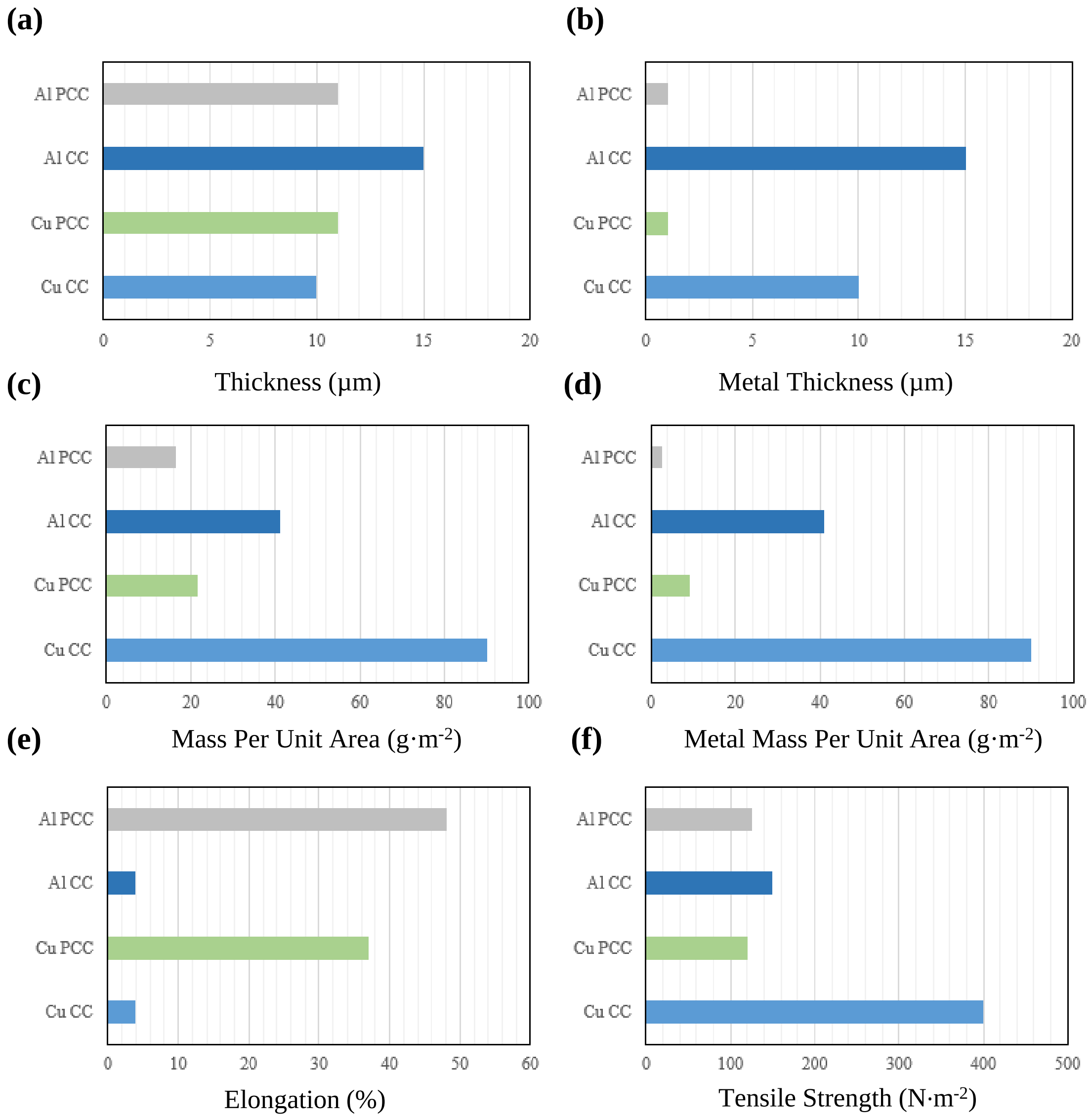

PCCs: Cell Groups and CT

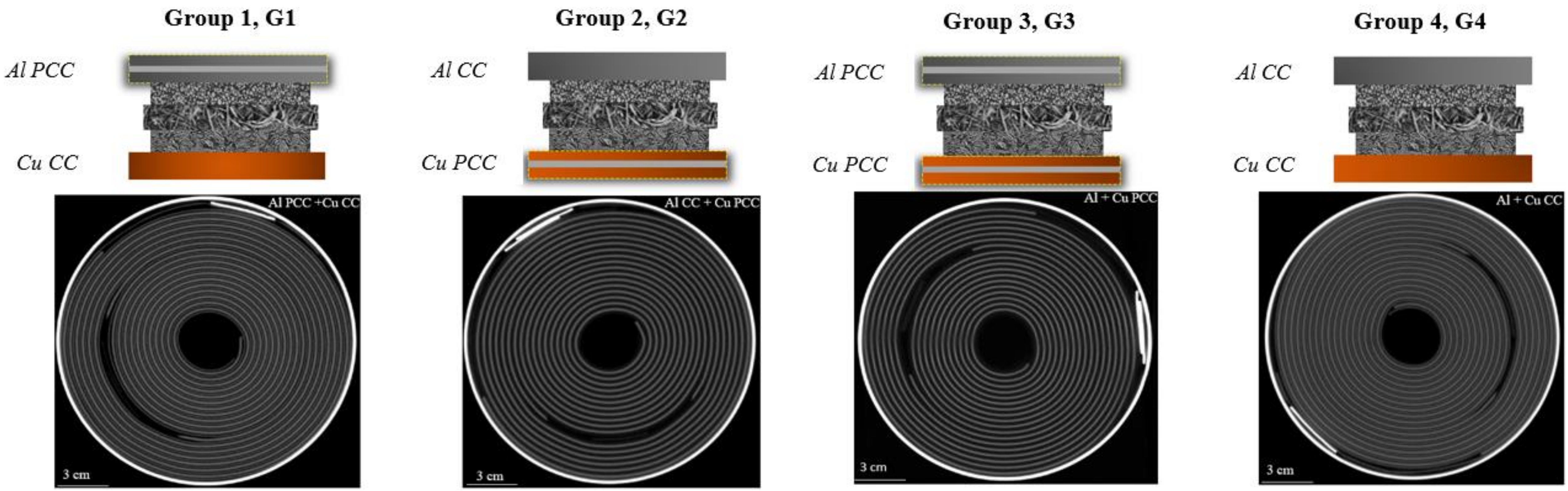

Results: Failure Prevention and Calorimetry

- Mass reduction in cells with one or both of the PCCs, mass reduction of 2.2 g with both

- Significant difference in observed TR output energy, maximum nail TC temperature and net cell mass loss with Al PCC cells

- Cu PCC alone did not protect the cells from undergoing thermal runaway but mitigation of the output energy was observed. This was due to the nail in contact with the cell during penetration, thus the Cu PCC despite protecting the anode, the graphite was connected to the cell can and shorted with the unprotected cathode.

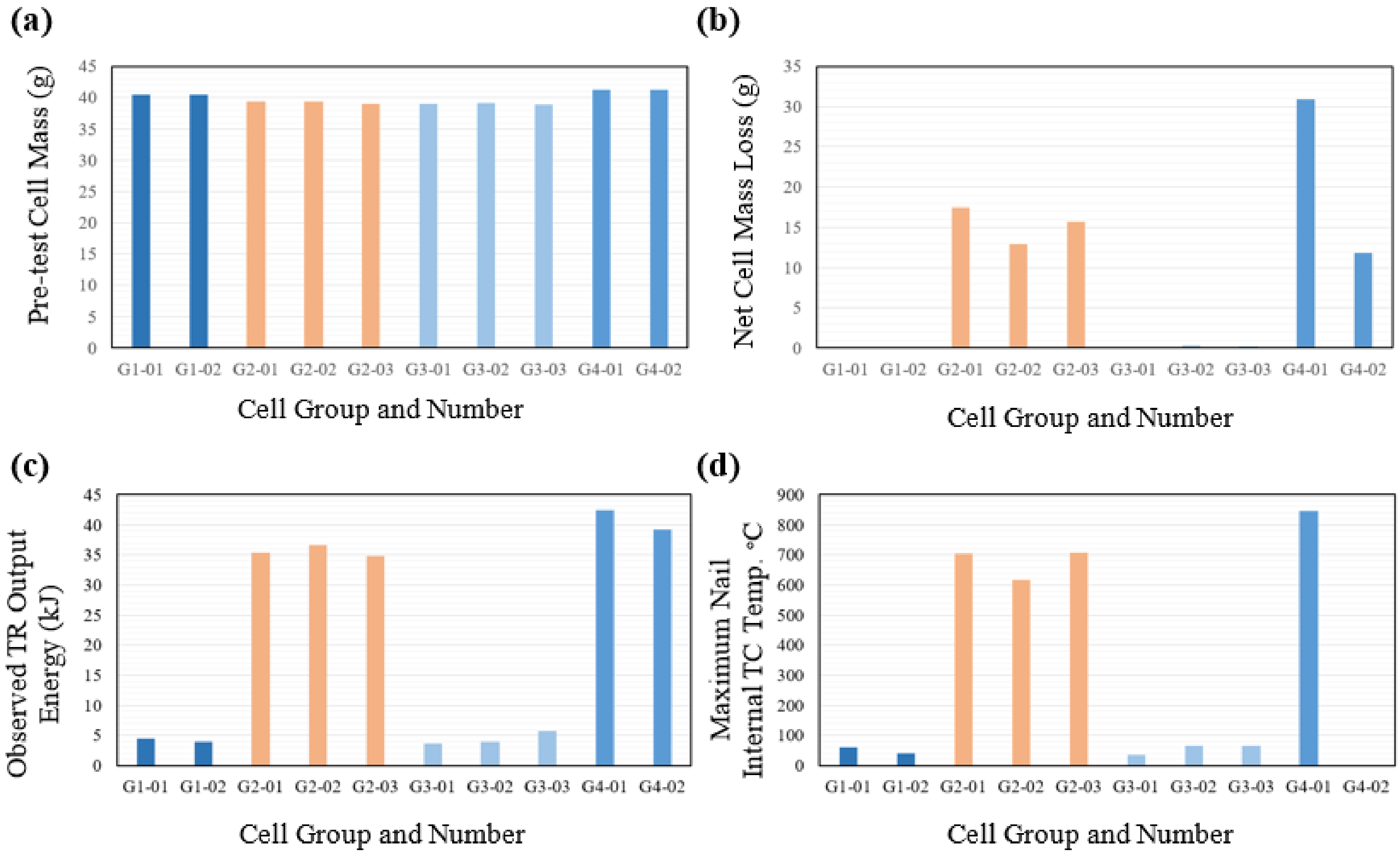

Results: Synchrotron X-ray Radiography

(a) G4-01 (Al CC + Cu CC) Radiography

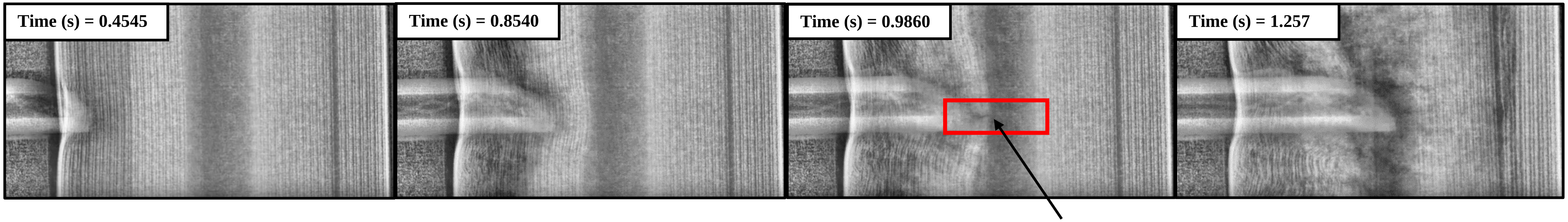

Characteristic cracking when Al PCC is absent

(b) G1-01 (Al PCC + Cu CC) Radiography

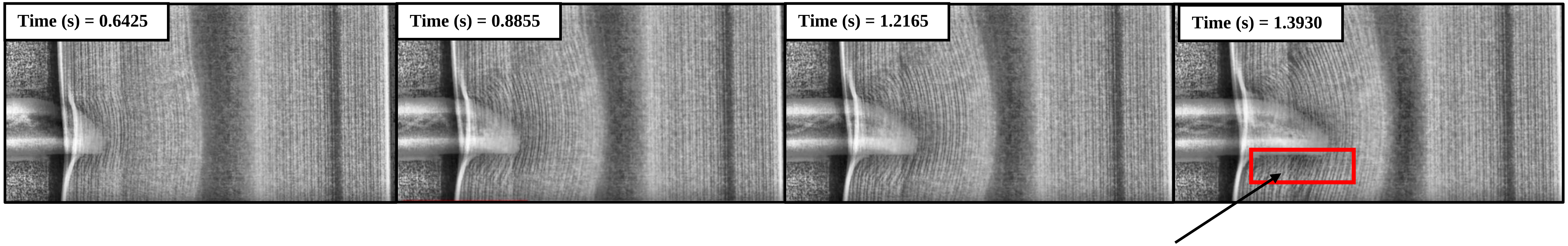

Electrode layers adjacent to nail splitting

Results: Post-mortem CT and 4.077 V

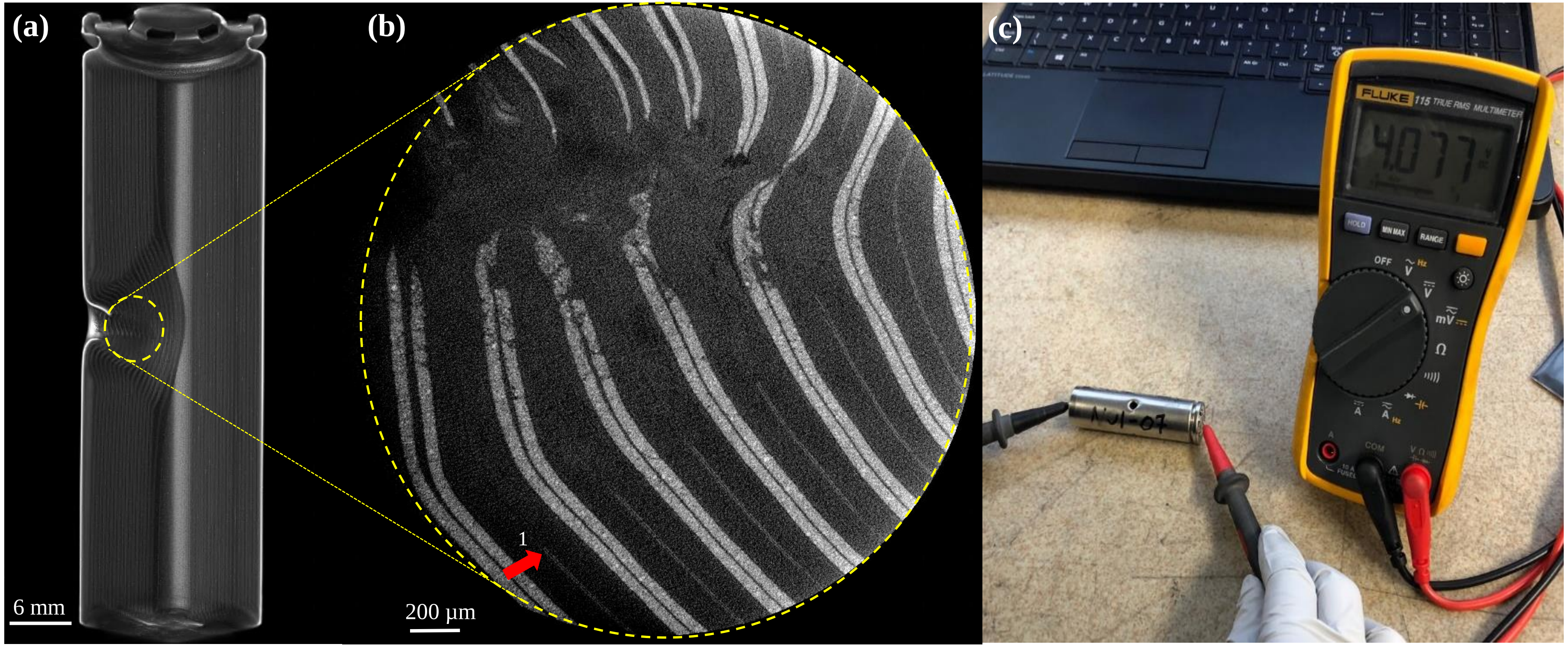

Sub-micron X-ray CT reveal Al PCC had shrunk away from the elevated temperature of the nail, which caused the microscopic short-circuit. This prevented further short-circuiting, subsequent OCV measurement showed 4.077 V. Cells retained voltage for over 10 months.

Conclusions

- High-speed X-ray imaging useful for **guiding and validating thermal runaway models** for identifying internal and external hotspots.
- Highest surface temperatures and **lowest burst pressures were achieved when initiation occurred near either ends of the cell,** due to relatively poor heat dissipation.
- The likelihood of high-risk failure scenarios can be increased by **selectively locating** the point of thermal runaway initiation within a cell.
- Thermal data from the fractional thermal runaway calorimeter (FTRC) is useful for accurately modelling efficacy of heat sinks and enclosures for withstanding thermal runaway.
- An **open-source database** of radiography and thermal data to be released soon.
- Acoustic technique demonstrated to enable detection of deformed electrode layers leading up to thermal runaway.
- Soteria's polymer substrate current collectors demonstrated to **withstand nail penetration without thermal runaway** where otherwise thermal runaway consistently occurs. Light-weight, cost effective, and mechanically robust for scaling up.

Thank you for listening

Donal Finegan
donal.finegan@nrel.gov

List of relevant publications:

1. Finegan et al., Characterising thermal runaway within lithium-ion cells by inducing and monitoring internal short circuits. *Energy & Environmental Science* **2017,** *10* (6), 1377-1388.
2. Finegan et al., Identifying the Cause of Rupture of Li-Ion Batteries during Thermal Runaway. *Advanced Science*, 1700369, **2017**.
3. Finegan et al., In-operando high-speed tomography of lithium-ion batteries during thermal runaway. *Nature Communications* **2015,** *6*.
4. Finegan et al., Tracking Internal Temperature and Structural Dynamics during Nail Penetration of Lithium-Ion Cells. *Journal of The Electrochemical Society* **2017,** *164* (13), A3285-A3291.
5. Finegan et al., Modelling and experiments to identify high-risk failure scenarios for testing the safety of lithium-ion cells, *J. of Power Sources*, **2019**
6. Walker et al., Decoupling of heat generated from ejected and non-ejected contents of 18650-format lithium-ion cells using statistical methods, *J. Power Sources*, **2019**
7. Robinson et al., Spatially Resolved Ultrasound Acoustic Investigations of Li-Ion Batteries, *Phys. Chem. Chem. Phys.*, **2019**
8. Pham et al., Correlative acoustic time-of-flight spectroscopy and X-ray imaging to investigate gas-induced delamination in lithium-ion pouch cells during thermal runaway, *J. Power Sources*, **2020**

www.nrel.gov

NREL
NATIONAL RENEWABLE ENERGY LABORATORY